THE ADSORPTION OF FATTY ACIDS USING METAL SILICA COMPLEXES FROM RICE HUSK ASH

CHUA JOO HANN

UNIVERSITI SAINS MALAYSIA

2008

THE ADSORPTION OF FATTY ACIDS USING METAL SILICA COMPLEXES FROM RICE HUSK ASH

by

CHUA JOO HANN

Thesis submitted in fulfillment of the requirements for the degree of Master of Science

May 2008

ACKNOWLEDGEMENTS

I would like to take this opportunity to thank Universiti Sains Malaysia especially the School of Chemical Sciences for giving me an opportunity to further my studies.

Prof. Madya Dr. Farook Adam, my supervisor, played an important role in my study. His advice, support, and encouragement, made my research progress smoothly. I would like to take this opportunity to thank Prof. Madya Dr. Farook Adam for helping me in the fulfillment of this study.

I would also like to thank the lab assistants, Mr. Aw Yong, Mr. Kanthasamy, Mr. Karuna, Mr. Muthu, and Madam Jamilah, in the FTIR and UV-Vis analyses, nitrogen adsorption analyses, XRD studies, TEM, and SEM and EDX analyses, respectively.

I would like to extend my heartfelt thanks to Mr. Adil Elhag Ahmed, Mr. Lim Ee Ju and Mr. Ooi Cheng Aik for knowledge sharing, spiritual supports, and endless help. Finally, my sincere thanks to my family members for tireless encouragement, endless love, understanding and financial support.

TABLE OF CONTENTS

	Page
ACKNOWLEDGEMENTS	ii
TABLE OF CONTENTS	iii
LIST OF TABLES	vii
LIST OF FIGUES	viii
LIST OF ABBREVIATIONS	x
LIST OF SYMBOLS	xi
LIST OF APPENDICES	xiii
LIST OF PUBLICATIONS AND SEMINARS	xiv
ABSTRAK	xv
ABSTRACT	xvii
CHAPTER 1 – INTRODUCTION	
1.1 Introduction	1
1.2 Free fatty acids	2
1.3 Silica extracted from rice husk ash (RHA)	3
1.4 Recent development in the use of researches of RHA	5
1.5 Sol-gel chemistry	7
1.5.1 General trends of sol-gel reaction under acidic and basic conditions	9
1.5.1.1 Sol-gel reaction under acidic conditions (e.g. with mineral acids)	9
1.5.1.2 Sol-gel reaction under basic conditions (e.g. with ammonia)	10

1.6 Principles of Adsorption 11

1.6.1 Introduction 11

1.6.2 Adsorption at the gas/solid interface 12

1.6.2.1 Classification of pores 12

1.6.2.2 Classification of adsorption isotherms 13

1.6.2.3 IUPAC classification of adsorption-desorption hysteresis loops 16

1.6.2.4 Brunauer-Emmett-Teller (BET) surface area determination 18

1.6.3 Adsorption at the liquid /solid interface 20

1.6.3.1 Adsorption Equilibrium 20

1.6.3.2 Langmuir Isotherm 20

1.6.4 Adsorption Thermodynamics 22

1.7 Objectives 25

CHAPTER 2 – METHODOLOGY

2.1 Synthesis of metal-silica complexes from RHA 27

2.1.1 Preparation of rice husk ash 27

2.1.2 Acid washing 27

2.1.3 Silica extraction 28

2.1.4 Production of metal-silica complexes 28

2.2 Sample characterization 29

2.2.1 Fourier Transform Infrared Spectra (FTIR) 29

2.2.2 UV-vis spectroscopy 29

2.2.3 Scanning Electron Microscopy (SEM) 29

2.2.4 Energy Dispersive X-ray Spectrometry (EDX) 30

2.2.5 Transmission Electron Microscopy (TEM) 30

2.2.6 Powder X-ray Diffractometry (XRD) 31

2.2.7 Nitrogen adsorption 31

2.3 Adsorption study of fatty acids on adsorbents 32

2.3.1 Reagents preparation 32

2.3.2 The interaction between adsorbents and solvent 33

2.3.3 Batch Adsorption Procedures 33

2.3.4 Studies on the possible interactions occurred between the adsorbent-adsorbate. 34

2.3.5 Acetone elution on adsorbents 34

CHAPTER 3 – RESULTS AND DISCUSSION

3.1 Characterization 35

3.1.1 Fourier Transform Infrared Spectra (FTIR) 35

3.1.2 UV-vis Spectroscopy 37

3.1.3 Energy Dispersive Spectrometry (EDX) 39

3.1.4 Scanning Electron Microscopy (SEM) 42

3.1.5 Powder X-ray Diffractometry (XRD) 43

3.1.6 Transmission Electron Microscopy (TEM) 44

3.1.7 Nitrogen Adsorption 46

3.2 Adsorption studies 50

3.2.1 Effect of metal incorporation onto silica gel 50

3.2.2 Effect of temperature 53

3.2.3 Thermodynamic study 54

3.3 Structure and orientation of fatty acids adsorbed onto adsorbent 59

3.3.1 The interaction between adsorbents and solvent 59

3.3.2 The interaction between adsorbent-adsorbate 60

3.3.3 Acetone elution on adsorbents 68

CHAPTER 4 – CONCLUSION 70

4.1 Conclusion 70

BIBLIOGRAPHY 73

APPENDICES 80

PUBLICATIONS & SEMINARS 84

LIST OF TABLES

		Page
Table 1.1	IUPAC Pore Classification.	13
Table 1.2	Classification of Microporosity.	13
Table 1.3	The effects of the enthalpy and entropy and the effect of temperature on spontaneity.	24
Table 3.1	Assignment of FTIR bands of commercial silica, RHA-SiO_2, RHA-Co, RHA-Ni, RHA-Cu and RHA-Zn.	35
Table 3.2	The results of nitrogen adsorption analyses.	49
Table 3.3	Langmuir constants and other derived parameters for the adsorption of lauric, stearic and oleic acid onto commercial silica, RHA-SiO_2, RHA-Co, RHA-Ni, RHA-Cu and RHA-Zn, at 303 K, 313 K and 323 K.	52
Table 3.4	The adsorption capacity, q_m, for the adsorption of fatty acids onto the commercial silica, RHA-SiO_2, RHA-Co, RHA-Ni, RHA-Cu and RHA-Zn.	54
Table 3.5	Thermodynamic heats of adsorption of lauric acid on commercial silica, RHA-SiO_2, RHA-Co, RHA-Ni, RHA-Cu and RHA-Zn.	56
Table 3.6	Thermodynamic heats of adsorption of stearic acid on commercial silica, RHA-SiO_2, RHA-Co, RHA-Ni, RHA-Cu and RHA-Zn.	57
Table 3.7	Thermodynamic heats of adsorption of oleic acid on commercial silica, RHA-SiO_2, RHA-Co, RHA-Ni, RHA-Cu and RHA-Zn.	58

LIST OF FIGURES

		Page
Fig. 1.1(a)	Acid-catalyzed silica structure which yield primarily linear or randomly branced polymer.	11
Fig. 1.1(b)	Based-catalyzed which yield highly branch clusters.	11
Fig. 1.2	The six types of adsorption isotherm, I to VI, in the IUPAC classification [52].	16
Fig. 1.3	The IUPAC classification of hysteresis loops [53].	17
Fig. 3.1	The FTIR spectra of commercial silica, RHA-SiO_2, RHA-Co, RHA-Ni, RHA-Cu, and RHA-Zn.	36
Fig. 3.2	UV-vis spectra of RHA-Co, RHA-Ni, and RHA-Cu.	38
Fig. 3.3	The EDX results for (a) Commercial silica, (b) RHA-SiO_2, (c) RHA-Co, (d) RHA-Ni, (e) RHA-Cu, and (f) RHA-Zn.	41
Fig. 3.4	The SEM micrographs of (a) commercial silica, (b) RHA-SiO_2, (c) RHA-Co, (d) RHA-Ni, (e) RHA-Cu, (f) RHA-Zn at × 10k magnification.	42
Fig. 3.5	The XRD results for (a) Commercial silica, (b) RHA-SiO_2, (c) RHA-Co, (d) RHA-Ni, (e) RHA-Cu, and (f) RHA-Zn.	43
Fig. 3.6	The TEM micrographs of (a) commercial silica, (b) RHA-SiO_2, (c) RHA-Co, (d) RHA-Ni, (e) RHA-Cu, (f) RHA-Zn.	45
Fig. 3.7	Nitrogen adsorption-desorption isotherm of (a) Commercial silica, (b) RHA-SiO_2, (c) RHA-Co, (d) RHA-Ni, (e) RHA-Cu, and (f) RHA-Zn	47
Fig. 3.8	Pore size distribution of (a) Commercial silica, (b) RHA-SiO_2, (c) RHA-Co, (d) RHA-Ni, (e) RHA-Cu, and (f) RHA-Zn	48
Fig. 3.9	The Langmuir linear plot of lauric acid adsorbed onto the adsorbents at 30 ºC.	51

Fig. 3.10	The FTIR spectra of commercial silica, RHA-SiO2, RHA-Co, RHA-Ni, RHA-Cu, and RHA-Zn after treating with isooctane.	59
Fig. 3.11	FTIR spectra of lauric acid adsorbed on (a) RHA-Co, (b) RHA-Ni, (c) RHA-Cu, (d) RHA-Zn, with their clean adsorbents subtracted and (e) Pure lauric acid.	63
Fig. 3.12	FTIR spectra of stearic acid adsorbed on (a) RHA-Co, (b) RHA-Ni, (c) RHA-Cu, (d) RHA-Zn, with their clean adsorbents subtracted and (e) Pure strearic acid.	64
Fig. 3.13	FTIR spectra of oleic acid adsorbed on (a) RHA-Co, (b) RHA-Ni, (c) RHA-Cu, (d) RHA-Zn, with their clean adsorbents subtracted and (e) Pure oleic acid.	65
Fig. 3.14	UV-Vis spectra of (a) RHA-Co, and RHA-Co adsorbed with (b) lauric acid, (c) stearic acid, (d) oleic acid.	66
Fig. 3.15	UV-Vis spectra of (a) RHA-Ni, and RHA-Ni adsorbed with (b) lauric acid, (c) stearic acid, (d) oleic acid.	66
Fig. 3.16	UV-Vis spectra of (a) RHA-Cu, and RHA-Cu adsorbed with (b) lauric acid, (c) stearic acid, (d) oleic acid.	67
Fig. 3.17	The probable surface complex formed involving (a) The fatty acid is bonded via the un-dissociated carbonyl group to the surface hydroxyl group; (b) The carbonyl oxygen of the fatty acid is attached directly to the metal center. (M= Co, Ni, Cu, Zn).	68
Fig. 3.18	The FTIR spectra of acetone-washing-adsorbents after stearic acid adsorption.	69

LIST OF ABBREVIATIONS

RHA	-	Rice husk ash
SiO_2	-	Silica
–Si–O–Si–	-	Siloxane
Si–OH	-	Silanol
BJH	-	Barret, Joyner and Halenda
IUPAC	-	The International Union of Pure and Applied Chemistry
BET	-	Brunauer, Emmett and Teller
STP	-	Standard temperature & pressure
RHA-SiO_2	-	Silica extracted from rice husk ash
RHA-Co	-	Silica incorporated with Co(II)
RHA-Ni	-	Silica incorporated with Ni(II)
RHA-Cu	-	Silica incorporated with Cu(II)
RHA-Zn	-	Silica incorporated with Zn(II)
FTIR	-	Fourier Transform Infrared
UV-Vis	-	Ultraviolet-visible
SEM	-	Scanning Electron Microscopy
EDX	-	Energy Dispersive X-ray Spectrometry
TEM	-	Transmission electron microscopy
XRD	-	Powder X-ray Diffractometry
DLVO	-	Derjaguin-Landau-Vervey-Overbeck
IEP	-	Isoelectric point

LIST OF SYMBOLS

P	-	Absolute pressure inside sample chamber (mm Hg)
P_o	-	Vapor presure of gas at sample temperature (mm Hg)
V	-	Volume of gas adsorbed per gram of material at STP (cc/g @ STP)
V_m	-	Volume of gas adsorbed corresponding to one monolayer on solid surface per gram (cc/g @ STP)
C	-	Constant
P/P_o	-	Relative pressure
S_{BET}	-	Specific surface area ($m^2\ g^{-1}$)
A_m	-	Area occupied by the adsorbed molecule in the monolayer ($mg\ g^{-1}$)
N	-	Avogadro's number.
C_e	-	Equilibrium concentration of adsorbate ($mg\ mL^{-1}$)
q_e	-	Amount of adsorbate adsorbed onto the adsorbent at equilibrium ($mg\ g^{-1}$)
q_m	-	Monolayer adsorption capacity ($mg\ g^{-1}$)
K_A	-	Langmuir adsorption equilibrium constant ($ml\ mg^{-1}$).
C_o	-	Initial concentration of the adsorbate ($mg\ mL^{-1}$)
V	-	Volume of solution (mL)
m	-	The weight of solid adsorbent (g)
R_L	-	Equilibrium parameter
ΔG^o_{ads}	-	Gibbs free energy change ($kJ\ mol^{-1}$)
ΔH^o_{ads}	-	Enthalpy ($kJ\ mol^{-1}$)

ΔS^{o}_{ads}	-	Entropy (J mol^{-1})
R	-	Universal gas constant, 8.314 J/(mol K)
K_o	-	Thermodynamic equilibrium constant (kg^{-1})
T	-	Temperature (K)
υ_s	-	Activity coefficient of the adsorbed solute
υ_e	-	Activity coefficient of the adsorbed solute in equilibrium
($^{w}/_{w}$)	-	Ratio of weight to weight
M	-	Molarity
Å	-	Angstrom
θ	-	Diffraction angle
r	-	Pearson's correlation coefficient

LIST OF APPENDICES

Page

Appendix A – Adsorption Isotherm Plot

A.1 The Langmuir linear plot of lauric acid adsorbed onto the adsorbents at (a) 30 ºC, (b) 40 ºC, and (c) 50 ºC. 80

A.2 The Langmuir linear plot of stearic acid adsorbed onto the adsorbents at (a) 30 ºC, (b) 40 ºC, and (c) 50 ºC. 81

A.3 The Langmuir linear plot of oleic acid adsorbed onto the adsorbents at (a) 30 ºC, (b) 40 ºC, and (c) 50 ºC. 82

A.4 The van't Hoff plot for the adsorption of (a) lauric acid, (b) stearic acid, and (c) oleic acid, onto the adsorbents. 83

LIST OF PUBLICATIONS & SEMINARS

	Page
1. Chua. J.H., Adam, F. "ADSORPTION STUDY OF FATTY ACID USING METAL-SILICA COMPLEXE FROM RICE HUSK ASH", article presented at the 1st Penang International Conference for Young Chemists, 2006, 24-27 May, Universiti Sains Malaysia, Penang.	85
2. Chua, J.H., Adam, F. "Adsorption of fatty acids using metal-silica complexes from rice husk ash", article presented at the 3rd Colloquium on Postgraduate Research, National Postgraduate Colloquium on Materials, Minerals and Polymers 2007 (MAMIP 2007), 2007, 10-11 April, Vistana Hotel, Penang.	86

PENJERAPAN ASID LEMAK DENGAN KOMPLEKS LOGAM SILIKA DARIPADA ABU SEKAM PADI

ABSTRAK

Co (II), Ni (II), Cu (II) dan Zn (II) telah berjaya dipadukan ke dalam silika daripada abu sekam padi melalui proses sol-gel untuk menghasilkan penjerap RHA-Co, RHA-Ni, RHA-Cu dan RHA-Zn masing-masing. Ini dapat dijelaskan melalui keputusan EDX. Nisbah logam: silikon adalah sebanyak 1: 9, 1: 7, 1: 24, dan 1: 178 masing-masing. Keputusan FTIR menunjukkan kehadiran kumpulan berfungsi yang sama untuk silika komersial, RHA-SiO_2, RHA-Co, RHA-Ni, RHA-Cu dan RHA-Zn. Mikrograf SEM menunjukkan semua sampel mempunyai permukaan yang berporos dan tiada kehadiran bucu-bucu yang tajam. Keputusan ini adalah sejajar dengan corak pembelauan sinar-X yang menunjukkan kehadiran struktur hablur. Penjerapan asid lemak atas silika yang diubahsuai telah ditinjau sebagai fungsi suhu tindak balas dan jisim logam-silika kompleks. Data eksperimen mematuhi persamaan Langmuir dengan nilai pemalar korelasi yang baik. Pemalar keseimbangan, R_L, menunjukkan semua sampel bertindak sebagai penjerap asid lemak yang baik. Tenaga bebas penjerapan Gibbs, ΔG^{o}_{ads}, yang diperolehi bernilai antara -30 dan -37 kJ mol^{-1}, manakala untuk ΔH^{o}_{ads} dan ΔS^{o}_{ads} adalah bernilai antara -12 dan -32 kJ mol^{-1}, dan antara +15 dan +70 J mol^{-1}, masing-masing. Parameter termodinamik yang diperolehi menunjukkan proses penjerapan merupakan proses eksotermik. Nilai negatif untuk tenaga bebas penjerapan Gibbs menunjukkan proses penjerapan

yang dijalankan merupakan proses yang digemari dan berlaku secara spontan. Spektra FTIR untuk asid lemak yang telah dijerap atas silika gel yang diubahsuai menunjukkan oksigen karbonil untuk acid lemak bebas telah berinteraksi dengan kumpulan hidroksil pada permukaan silika. Daripada spektra UV-Vis, penganjakan jalur d-d untuk gel silika yang diubahsuai menunjukkan asid lemak telah berinteraksi secara terus dengan pusat logam.

THE ADSORPTION OF FATTY ACIDS USING METAL SILICA COMPLEXES FROM RICE HUSK ASH

ABSTRACT

Co (II), Ni (II), Cu (II) and Zn (II) were successfully incorporated into silica from rice husk ash (RHA) via a simple sol-gel process to yield the adsorbents RHA-Co, RHA-Ni, RHA-Cu and RHA-Zn respectively. This was shown by EDX. The metal: silicon ratio was found to be 1: 9, 1: 7, 1: 24, and 1: 178 respectively. FTIR showed the presence of similar functional groups for commercial silica, RHA-SiO_2, RHA-Co, RHA-Ni, RHA-Cu and RHA-Zn. SEM micrographs showed all samples had porous surface and no sharp edges were observed. These results were consistent with the X-ray diffraction patterns, which showed their amorphous nature. The adsorption of fatty acid on the modified silica was investigated in a batch system, as a function of reaction temperature and the mass of metal-silica complex. The experimental data fitted well to the Langmuir equation, with good correlation coefficients. The equilibrium parameter, R_L, revealed that all samples were good adsorbents for these fatty acids. The Gibbs free energy of adsorption, ΔG^{o}_{ads}, was found to be between -30 to -37 kJ mol^{-1}, while ΔH^{o}_{ads} and ΔS^{o}_{ads} were found to be between -12 to -32 kJ mol^{-1} and +15 to +70 J mol^{-1} respectively. Thermodynamic parameters obtained showed the adsorption process was exothermic in nature. The negative Gibbs free energy values obtained showed the on-going adsorption process was favorable as well as spontaneous. The FTIR spectra of fatty acids adsorbed on the modified silica

gel showed that the carbonyl oxygen of the free fatty acid was attached to the silica surface hydroxyl group. From the UV-Vis spectra, the shifts of the d-d bands of the modified silica gel indicated that the fatty acids had interacted directly with the metal center.

Chapter 1

Introduction

1.1 Introduction

In 1997, there was a massive environmental issue which occurred in Southeast Asia – air pollution generated by vegetation fires in Indonesia. Between July and November 1997, it was estimated that 45,000 km^2 of forest and land were burnt on the islands of Sumatra and Kalimantan. The emissions of these fire caused considerable air pollution throughout the Southeast Asian region, notably in Indonesia, Malaysia and Singapore [1].

A similar problem is encountered in the rice milling industry. Rice husk, a form of agricultural biomass, is generated in large quantities as a major by-product in the rice milling industry in Southeast Asia. The local annual production of rice leaves behind about 2.4 million tones of husk as waste product [2]. The amount of rice husk available is far in excess for any local uses, and thus frequently causing disposal problems. Uncontrolled burning is often considered the most effective disposal method for such by-product. The partially burnt rice husk in turn contributed to environment pollution which may cause acute and chronic respiratory diseases such as asthma, upper respiratory infection, bronchitis, decreased lung function, eye and skin irritation. Besides health impacts, this issue also seriously affected the economies of these regions, ranging from air, land and sea transportation, to construction and tourism. Hence, alternative solutions to dispose the rice husk should be explored to overcome these problems.

1.2 Free fatty acids

Fatty acid is an important industrial material in the oleochemical industry, for the production of various important oleochemicals such as fatty alcohols, soaps, drugs, plastics, lubricants, and other detergents [3], which are widely used in the pharmaceutical and food industry. Free fatty acids in vegetable oils resulted from the breaking of the triglyceride ester bonds, are normally removed during the refining process in the industry. Wastewater containing fatty acids is produced from diverse industrial sources, such as food processing industries, vegetable oil refineries, and domestic sewage. Fatty acids substances which arise from the decay of plant and animal residues exist as a heterogeneous mixture of organic materials in soils, drains, rivers, and sea.

The presence of fatty acids in water streams has become an environmental problem due to their harmful effects on human being, aquatic life, and on the flora and fauna. Therefore the research for methods to remove free fatty acid from contaminated aquatic systems is deemed important for the protection of environmental health.

Adsorption has been proved to be an excellent way to treat fatty acid effluents, offering significant advantages such as the cheapest, easy availability, easy operation and efficiency, comparing to many conventional methods especially from the economical and environmental point of view [4]. Thus, the adsorbent properties of zeolites [5], clays [6], fibers [7], activated carbon [8], membranes [9,

10], chitosan [11], and ion exchange resin [12] were studied and utilized in a wide range of applications, such as wastewater treatment and clarification of fat and oil. The most generally used solid adsorbent is activated carbon which is a very efficient solid adsorbent in many different applications due to their high surface area, high efficiency, easy operation, with chemical, radiation and thermal stability [13]. However the activated carbon is expensive and very costly [14]. Therefore, the needs for an alternative low-cost absorbent, have encouraged the research for new and cheap sources in aqueous effluent treatment.

Several alternative materials from natural resources had been proposed. In this context, natural material including by-products and wastes from agricultural and forest industries had been studied. Some common waste materials used for this purpose are, rice bran, coir pith, wheat bran, rubber wood sawdust, de-oiled soya, oil palm ash, and bagasse fly ash [15–21]. These could be assumed as low-cost materials since they require little processing, abundant in nature, and could be used either directly or after an activation treatment.

1.3 Silica extracted from rice husk ash (RHA)

Earlier research has shown that rice husk was composed of 20% ash, 38% cellulose, 22 % lignin, 18% pentose and 2% of other organic components [22]. The silica, SiO_2, content of the ash was more than 94% [23]. Various metal oxide, such as Na_2O, K_2O, CaO, MgO, Fe_2O_3 and MnO_2 [24] and unburned carbon influenced the purity and color of the ash. Silica is known to be one of the main precursors in

the ceramic industry and glassware manufacturing. It is widely used in pharmaceutical products, detergents, adhesives, desiccants, catalytic supports, chromatography column packing, and vegetable oil refining [25, 26].

Generally, two prime methods are used for the manufacture of amorphous silica [27]: (1) precipitation from aqueous solution of sodium silicate, and (2) high-temperature oxidation or hydration of silicon tetrachloride. The former will be referred to as precipitated silica or silica gel, while the latter will be referred to as silica fume. The main difference between these two types of silica is that silica gels can have a great diversity of micro- and mesoporosity, whereas, silica fumes are nonporous.

The solubility of amorphous silica is very low at pH < 10 and is increases at pH > 10. This unique behavior enables amorphous silica from RHA to be extracted in pure form using low temperature alkali extraction by solubilizing the RHA in alkaline solution followed by precipitation at a lower pH [24]. Generally, sodium silicate, the precursor for silica production, is manufactured by smelting quartz sand with sodium carbonate at 1300 ºC [28]. The extractable amorphous silica from RHA is cost effective, which provides a low energy method as an alternative to the current high energy method.

Amorphous silica can be prepared by acidification of basic aqueous silicate solution as in reaction 1.1, and when reaction conditions are properly adjusted,

porous silica gels are obtained. Two types of chemical reactions are involved: silicate neutralization producing silicic acids (reaction 1.2), followed by condensation polymerization of the silicic acids (reaction 1.3).

$$Na_2SiO_3 + 2H^+ \xrightarrow{H_2O} SiO_2 + H_2O + 2Na^+ \qquad (1.1)$$

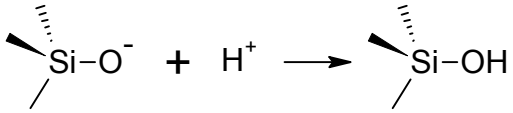

(1.2)

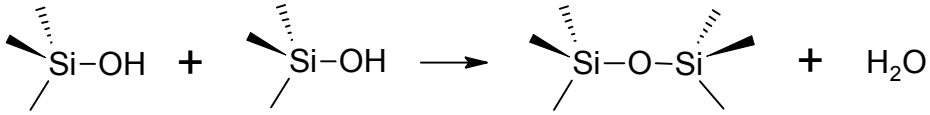

(1.3)

The morphology and the surface properties of the silica gel are dependent on the synthesis and treatment conditions. At higher pH, covalent siloxane bonds were predominant, the gel formation was rapid, and very rigid gels were formed; whereas, at lower pH, weaker Van der Waals attraction and hydrogen bonding (resulted from the presence of silanol (Si–OH) groups) were the major contributing forces for the silica network interaction.

1.4 Recent development in the use of researches of RHA

Rice husk ash (RHA), an agricultural biomass, has been extensively investigated due to the growing concern with environmental pollution. Adam et al. [29] had prepared and characterized silica gel from RHA and reported that it was comparable with commercial silica gel. Kalapathy et al. [30] had produces flexible self-supported films from RHA silica and showed that silicate existed in an

amorphous form in the film. The large amount of silica freely obtained from this source provides an abundant and cheap alternative of silica for many industrial usage, including as a cheap source for the preparation of zeolite [31], cement [32], concrete [33], and cordierite [34] synthesis. Arayapranee et al. [35] had incorporated the RHA into natural rubber, and claimed that the hardness of the resulting rubber increased and could be used as the cheaper filler for natural rubber materials.

Other than that, the application of RHA as a catalyst support had been extensively studied to meet the demand for high melting point, high metal dispersion and high surface area by Chang et al. [36, 37] and Adam et al. [38]. They reported that RHA was found to be a preferable catalyst support over silica gel. Feng et al. [39] studied the removal of heavy metal in aqueous solution by RHA and claimed that the adsorption rate and capacity of RHA were considerably higher and faster than many other materials.

The adsorption properties of silica had been much studied because of their great practical importance and the widespread of industrial use in silica materials. Saleh and Adam [40] had investigated the adsorption isotherms of lauric, myristic and stearic acid on RHA and they showed the adsorption studied conformed to Langmuir isotherm. They also reported that the fatty acids adsorbed onto RHA could be easily eluted out by acetone and suggested that the adsorption of fatty acids took place by physisorption. Liew et al. [41] studied the adsorption of

carotene from crude palm oil on acid-activated RHA. They reported a rapid decrease in the residual carotene by adding unwashed acid-activated RHA. Proctor and Palaniappan [42] reported that the most effective RHA ashing temperature was 500 °C and the performance of acid-activated ash was comparable to that of activated bleaching earth in the soy oil lutein adsorption. They also demonstrated that free fatty acids from soybean oil could be adsorbed by RHA from a soybean oil/hexane miscella, which followed a Freundlich isotherm [43]. Kalapathy and Proctor [44] produced sodium silicate films from RHA and studied on their application in reducing the free fatty acids in frying oil. Chang et al. [45] reported that the acid activated RHA increase the bleaching efficiency of sesame oil and concluded that the replacement of activated clay by acid activated RHA was promising.

The research work discussed above not only provides a solution for waste disposal but also recovers a valuable silica product, together with certain useful associated improvements and the generation of value added product from agricultural waste. The use of RHA is on the rise based on the increasing number of publications appearing to date.

1.5 Sol-gel chemistry

To date, sol-gel methods have been used to synthesize a large number of metal-silica composites. These systems commonly contain the desired metal entrapped in the silica matrix, and therefore such materials contain silica as the

major phase. Metal-silica composites prepared by sol-gel chemistry are high surface area and high porosity materials which are attractive in many applications such as insulators, ceramic precursors, adsorbents, and catalyst supports [46].

Sol-gel chemistry is an attractive alternative to other synthetic methods for many reasons. The method is low temperature, low cost, versatile, and can generally be done under room conditions with general lab equipments, all of which making the preparing process to be convenient and inexpensive. In general, the sol-gel process involves the transition of a system from a liquid "sol" (mostly colloidal) into a solid "gel" phase. The starting materials used in the preparation of the "sol" are usually inorganic metal salts or metal organic compounds such as metal alkoxides. In a typical sol-gel process, the precursor is subjected to a series of hydrolysis and polymerization reactions to form a colloidal suspension, or a "sol". A three-dimensional cross-linked inorganic network structure can be developed in situ within a polymer matrix. The factors affecting the resulting silica network are as follows: pH, temperature and time of reaction, reagent concentrations, catalyst nature and concentration, H_2O/Si molar ratio, and aging period and temperature.

According to Iler [27], sol-gel polymerization occurs in three stages:

1. Polymerization of monomers to form particles.
2. Growth of particles.
3. Linking of particles into chains, then networks that extend throughout the liquid medium, thickening into a gel.

1.5.1 General trends of sol-gel reaction under acidic and basic conditions

Polymerization to form siloxane bonds occurs by condensation reaction. The rate of the polymerization is dependent on the environmental pH. Generally, under acid-catalyzed conditions, the yield is primarily linear or randomly branched polymers which entangle and form additional branches resulting in gelation. In contrast, silica networks derived under base-catalyzed conditions yield more cross-linked and highly branched clusters which do not interpenetrate prior to gelation and thus behave as discrete clusters (Fig. 1.1). Silica xerogel produced under relatively acidic conditions display type I nitrogen adsorption isotherm characteristic of microporous materials, whereas those produced under basic conditions display type IV isotherm characteristic of mesoporous materials. Since the isoelectric point of silica is ~ pH 2, the reactions are catalyzed by H^+ at pH < 2, while OH^- at pH > 2 [47].

1.5.1.1 Sol-gel reaction under acidic conditions (e.g. with mineral acids)

The condensation rate is proportional to the H^+ concentration [47]. The H^+ ion attached to oxygen in SiOH produces a transition state with a positive charge. The hydrolysis reaction is speeded up more efficiently than the condensation reaction. Condensation involves the attack of silicon atoms carrying protonated silanol species by neutral ≡Si-OH nucleophiles. Acidic conditions delay the formation of protonated silanol species, but inhibit some nucleophiles. The most basic silanol species (the most likely to be protonated) are those contained in monomers or weakly branched oligomers :

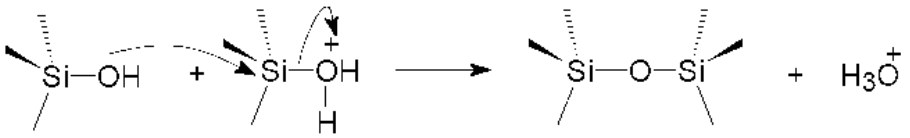

(1.4)

So a bushy network of weakly branched polymer is obtained.

1.5.1.2 Sol-gel reaction under basic conditions (e.g. with ammonia)

Condensation rate is proportional to OH^- concentrations [47]. Hydroxyl anions (OH^-) attached to Si produces a transition state with a negative charge. Hydroxyl anions (OH^-) and deprotonated silanol (≡Si-O^-) are better nucleophiles than water and silanol species due to an inductive effect. A fast attack at the silicon atom causes both hydrolysis and condensation reactions occur simultaneously. The condensation involves the attack of a deprotonated silanol (≡Si-O^-) on a neutral siloxane species:

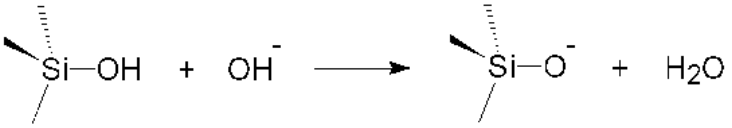

(1.5)

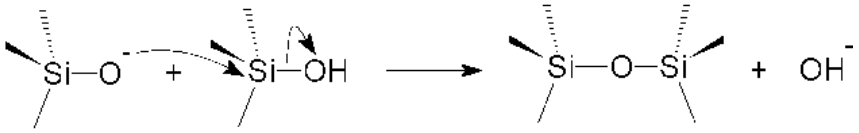

(1.6)

The result of basic catalysis is an aggregation (monomer-cluster) that leads to a more compact and highly branched silica networks which are not interpenetrable before drying and thus behave as discrete species.

(a) **(b)**

Fig. 1.1: (a) acid-catalyzed silica structure which yield primarily linear or randomly branced polymer; (b) based-catalyzed which yield highly branch clusters [28].

1.6 Principles of Adsorption

1.6.1 Introduction

Based on the bonding nature between the molecule and the surface, adsorption phenomena are divided into the two sub-categories: physisorption and chemisorption. In physisorption, no chemical bonds are formed and the attraction between the adsorbate and adsorbent exists by the formation of intermolecular electrostatic, such as Van der Waals forces from induced dipole-dipole interactions. These attractions to the surface are usually weak. The chemical identity of the adsorbate remains intact, i.e. no breakage of the covalent bonds of the adsorbate takes place.

In chemisorption, the adsorbate sticks to the solid by the formation of a chemical bond with the surface. This interaction is much stronger, and, in general, chemisorption has more stringent requirements for the compatibility of adsorbate

and surface site than physisorption. Chemisorption is far less common than physisorption. The regeneration of the chemical bonds formed for subsequent re-use is often difficult or impossible.

Adsorption at the gas/solid interface

Physical gas adsorption is often the first choice technique used to study the specific surface area and pore size distribution of powdered or solid materials. Nitrogen gas is ideal for measuring the surface area and pore size distribution. The dry sample is usually evacuated of all gases and cooled to the temperature of liquid nitrogen a 77 K. At this temperature nitrogen will physically adsorb on the surface of the sample. This adsorption process can be considered to be a reversible condensation or layering of molecules on the sample surface where heat is evolved. The isotherm obtained from these adsorption measurements provides information on the surface area, pore volume, and pore size distribution in the micro-, meso- and macroporosity range (approximately 0.5–200 nm) [48].

1.6.2.1 Classification of pores

The classical pore size model developed by Barret, Joyner and Halenda (BJH) [49] in 1951, which based on the Kelvin equation and corrected for multilayer adsorption, is most widely used for the evaluation of the mesopore size distribution and part of the macropore range. The International Union of Pure and Applied Chemistry (IUPAC) [50] have defined the porosity classification system, which

gives a guideline of pore diameter applicable to all forms of porosity. The widely accepted IUPAC classification is as follows:

Table 1.1: IUPAC Pore Classification.

Micropores	diameter < 2 nm
Mesopores	2 nm < diameter < 50 nm
Macropores	diameter > 50 nm

Microporosity may then be subdivided into three subsequent categories:

Table 1.2: Classification of Microporosity.

Ultramicropores	diameter < 0.5 nm
Micropores	0.5 nm < diameter < 1.4 nm
Supermicropores	1.4 nm < diameter < 2.0 nm

1.6.2.2 Classification of Adsorption Isotherms

Adsorption of a gas by a porous material is described quantitatively by an adsorption isotherm. An adsorption isotherm (at a fixed temperature) is usually recorded as a function of volume of gas adsorbed (cc/g @ STP) versus relative pressure, P/P_o (sample pressure / saturation vapor pressure). Isotherms provide a significant amount of information about the adsorbent used and the interaction with the adsorbate in the system, including assessment of the surface chemistry and fundamentals involved in the adsorption process, and estimation of the surface area, pore volume and pore size distribution of the adsorbate. The five hypotherical

types of physisorption isotherm originally proposed by Brunauer et al. [51] in 1940 were incorporated into a more practical classification by IUPAC [50] in 1985.

The IUPAC classification of adsorption isotherm is illustrated in Fig. 1.2. The six types of isotherms are the characteristics of adsorbents which are as follows:

Type I Isotherm – It is typical for microporous systems. It documents the adsorption of gas into micropores at very low gas pressures, which shows a fairly rapid rise in the adsorbed quantity with increasing pressure (or concentration) up to saturation. They are characterized by a plateau that is nearly or quite horizontal, resulting in the absence of mesopores. Adsorption into micropores is completely reversible and no hysteresis loop is observed because of the inability for the adsorbate to condense in such narrow volume elements.

Type II Isotherm – Monolayer coverage is followed by multi-layering at high relative pressures, which are normally obtained with non-porous adsorbents. It is associated with stronger fluid-solid interaction [52]. Nonporous samples show neither of the enhanced adsorption, but instead, resemble curves for nonporous standards (Type II isotherm, no hysteresis, no enhanced adsorption).

Type III Isotherm – It occurs when the forces of interaction between adsorbate and adsorbent are relatively small [52] and is most commonly associated with both non-porous and macroporous adsorbents. The weak interactions between the

fluid-solid lead to low uptakes at low relative pressures. However, once a molecule has become adsorbed at a primary adsorption site, the fluid-solid interaction, which is much stronger, becomes the driving force of the adsorption process, resulting in accelerated uptakes at higher relative pressure.

Type IV Isotherm – Typical of mesoporous systems. It is the result of surface coverage of the mesopore walls followed by pore filling. Generally show hysteresis [49] in the adsorption and desorption branches above P/P_o = 0.4, attributed to multilayer formation and, especially capillary condensation in mesopores.

Type V Isotherm – These isotherms are convex to the relative pressure axis and are the characteristics of weak adsorbate-adsorbent interactions [52]. These isotherms are indicative of microporous or mesoporous solids. The hysteresis loop exhibited is associated with capillary condensation.

Type VI Isotherm – The isotherm is due to the complete formation of monomolecular layers before progressing to a subsequent layer which commonly associated with non-porous or macroporous adsorbents.

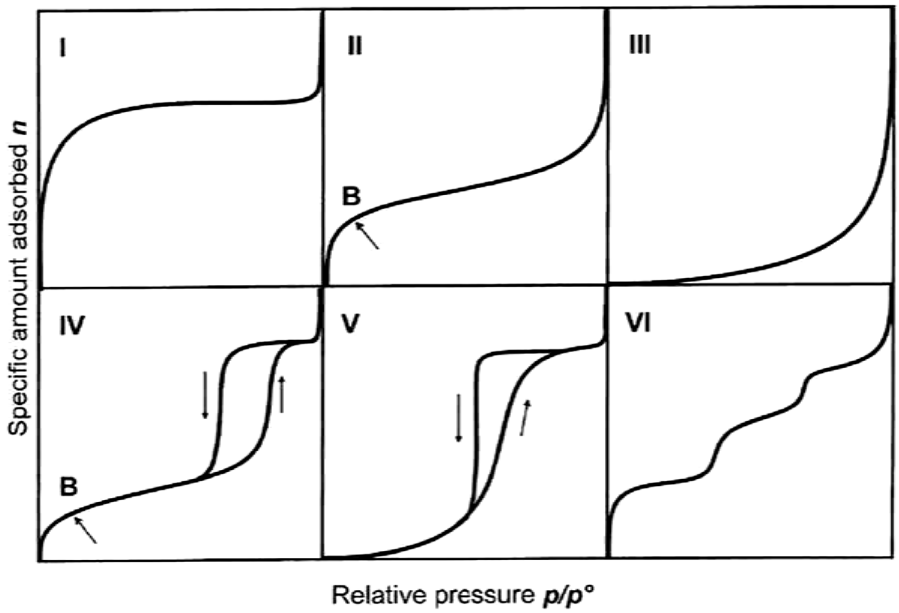

Fig. 1.2: The six types of adsorption isotherm, I to VI, in the IUPAC classification [52].

1.6.2.3 IUPAC classification of adsorption-desorption hysteresis loops

The adsorption process is generally taken as completely reversible, but, under some conditions the isotherm may exhibit a different shape upon desorption as compared to absorption. Hysteresis loops, which appear in the multilayer range of physisorption isotherms, are generally associated with pore filling (or capillary condensation) and pore emptying (or capillary evaporation) of mesopores. Adsorption isotherms in mesoporous materials exhibit two main typical features: (i) a sharp increase in the amount of gas adsorbed at a pressure lower than the bulk saturating vapor pressure P_o, whereby capillary condensation will occur and is preceded by a metastable fluid state (''cylindrical meniscus'') and (ii) when the pressure is decreased from P_o, the capillary evaporation occurs via a hemispherical meniscus, separating the vapor and the capillary condensed phase.

The size and shape of the loop itself gives a useful indication of the predominant pore filling emptying mechanism, and can be used to determine the structure and size of pores in the absorbent.

The IUPAC classification of hysteresis loops are represented in Fig. 1.3. In brief, H1 and H2 loops are typical for cylindrical pores, which H1 loops typical for homogeneous structure, whereas, H2 loop is typical for inhomogeneous structures. In contrast, H3 and H4 loops are typical for slit-like pores, which are typical for irregular and regular structures, respectively. An overview of the hysteresis loops is briefly described as below.

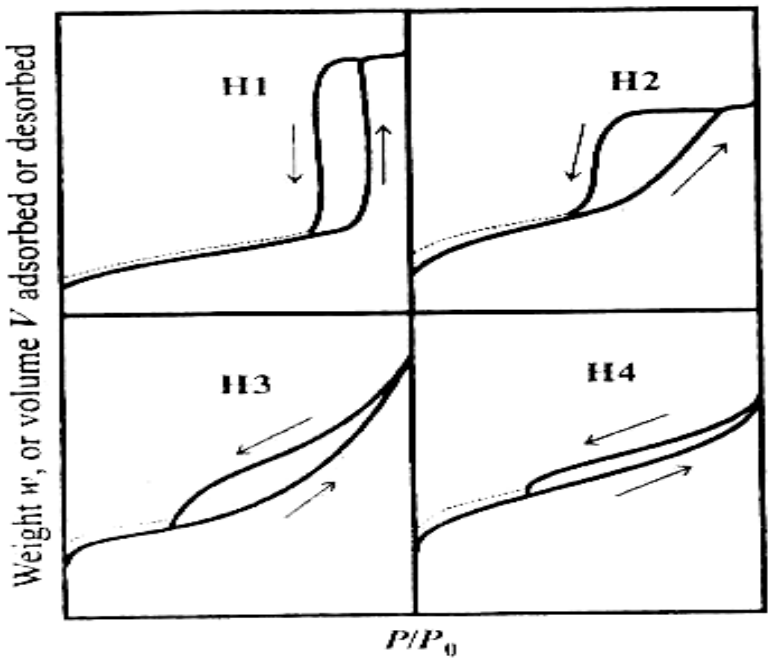

Fig. 1.3: The IUPAC classification of hysteresis loops [53].

Type H1 is a fairly narrow loop with a very steep and nearly parallel adsorption and desorption branches. It is given by adsorbents with a narrow

distribution of uniform pores, as well as with a well-organized and ordered porosity, which is generally associated with delayed condensation and very little percolation hold-up. In contrast, type H2 loop is broad with a long and almost flat plateau but with a steep desorption branch, which is given by adsorbents with a complex pore structure, made up of interconnected networks of pores of different sizes and shape.

Type H3 and H4 do not terminate in a plateau at high P/P_o, and the limiting desorption boundary curve is therefore more difficult to establish. Both of H3 and H4 loops do not close until the equilibrium pressure approaches the saturation pressure. Type H3 loops are usually given by the aggregates of platy particles or adsorbents containing slit-shaped pores. Hysteresis loops of type H4 are also given by slit-shaped pores with regular structure.

1.6.2.4 Brunauer-Emmett-Teller (BET) surface area determination

The BET equation derived by Brunauer, Emmett and Teller [54] is a well-known rule for the physical adsorption of gas molecules on a solid surface. Specific surface areas were deduced by applying BET theory for multilayer physisorption. The BET equation is used to give the volume of gas needed to form a monolayer on the surface of the sample. The actual surface area can be calculated with the knowledge of the size and number of the adsorbed gas molecules. The concept of the theory is an extension of the Langmuir theory [55], which is a theory for

monolayer molecular adsorption, to multilayer adsorption with the following hypotheses:

1. Adsorbent consists of a regular array of adsorption sites equal in energy, with a constant enthalpy of adsorption in the monolayer.
2. Adsorption is localized to these sites.
3. There is no interaction between each adsorption layer.
4. Gas molecules physically adsorb on a solid in layers infinitely.
5. Enthalpy of adsorption in second and subsequent multilayers is equal to the enthalpy of liquefaction.
6. Adsorption or desorption may only occur on or from exposed sites.

The resulting BET equation is expressed by (1.7):

$$\frac{P}{V(P_o \quad P)} = \frac{1}{V_m C} + \frac{(C \quad 1)P}{V_m C P_o} \tag{1.7}$$

where P = absolute pressure inside the sample chamber (mm Hg);

P_o = vapor pressure of gas at sample temperature (mm Hg);;

V = volume of gas adsorbed per gram of material at STP (cc/g @ STP);

V_m = volume of gas adsorbed corresponding to monolayer on solid surface (cc/g @ STP);

C = constant that depends on adsorbate, adsorbent, and temperature.

An adsorption isotherm plot of $P/V(P_o - P)$ versus P/P_o gives a straight line of slope $(C - 1)/V_mC$ and an intercept of $1/V_mC$ on the $P/V(P_o - P)$ axis. The BET

method is widely used in surface science for the calculation of surface area of solids by physisorption of gas molecules. The specific surface area, S_{BET}, is evaluated by the following equation:

$$S_{BET} = V_m A_m N. 10^{-18} \quad (1.8)$$

Where S_{BET} = specific surface area ($m^2 g^{-1}$);

A_m = area occupied by the adsorbed molecule in the monolayer ($mg g^{-1}$);

N = Avogadro's number.

1.6.3 Adsorption at the liquid-solid interface

1.6.3.1 Adsorption Equilibrium

Adsorption equilibrium is a dynamic concept which will be achieved when the rate at which molecules adsorb onto a surface which is equal to the rate at which they desorbed. Till now the statistical theories developed for gas – solid systems were applied for liquid – solid systems with little confidence for designing of the equipment. The most commonly used equilibrium model was Langmuir isotherm equation which is explained as follows.

1.6.3.2 Langmuir Isotherm

Adsorption isotherms describe how adsorbates interact with adsorbents and are critical in optimizing the use of adsorbents. Several adsorption isotherms have proven useful in understanding the adsorption process. The Langmuir isotherm [55] is the simplest isotherm which is attributed to as the pioneer in the

study of surface processes, and has been widely used to characterize the adsorption phenomenon, which is based on three major assumptions, these being:

1. The surface of the adsorbent is a two-dimensional array of energetically homogenous sites.
2. Only one molecule may be adsorbed on any one site and saturation of adsorption occurs at the monolayer coverage.
3. There are no interactions between any of the adsorbed molecules.

The linear form of the Langmuir adsorption equation can be represented as

$$\frac{C_e}{q_e} = \frac{C_e}{q_m} + \frac{1}{K_A\, q_m} \tag{1.9}$$

where C_e = equilibrium concentration of adsorbate in the solution (mg mL^{-1});

q_e = amount of adsorbate adsorbed on the adsorbent at equilibrium (mg g^{-1});

q_m = monolayer adsorption capacity (mg g^{-1});

K_A = Langmuir adsorption equilibrium constant (mL mg^{-1}), which is related to the energy of adsorption.

The monolayer capacity, q_m, is defined as the amount of adsorbate needed to cover the surface with a complete monolayer of molecules. q_m plays an important role in the comparison of adsorption efficiency as it expresses a practical limiting adsorption capacity when the surface is fully covered with adsorbate. By plotting C_e/q_e vs C_e, the values of q_m and K_A were determined from the slope and intercept

of the plot, respectively. Deviation from linearity may be due to structural effects, activated diffusion, molecular sieving effects or pore-filling effects.

The amount of adsorption at equilibrium, q_e (mg g^{-1}) was calculated according to the expression:

$$q_e = \frac{(C_o \quad C_e)V}{m} \tag{1.10}$$

where C_o = initial concentration of the adsorbate (mg mL^{-1});

V = volume of solution (mL);

m = the weight of solid adsorbent (g).

The essential characterization of the Langmuir equation can be expressed in terms of a separation factor or equilibrium parameter, R_L [56], which is defined as:

$$R_L = \frac{1}{1 + K_A C_o} \tag{1.11}$$

The R_L value indicates the shape of the isotherm to be either unfavorable ($R_L > 1$), linear ($R_L = 1$), favorable ($0 < R_L < 1$), or irreversible ($R_L = 0$).

1.6.4 Adsorption Thermodynamics

The changes in reaction that can be expected during the sorption process require the brief idea of thermodynamic parameters. The three main thermodynamic parameters include Gibbs free energy change (ΔG^o_{ads}), enthalpy

(ΔH^o_{ads}), and entropy (ΔS^o_{ads}). The Gibbs free energy change, ΔG^o_{ads}, can be determined using the relation as follows:

$$\Delta G^o_{ads} = RT \ln K_o \tag{1.12}$$

where R is the universal gas constant, 8.314 J/(mol K); K_o is the thermodynamic equilibrium constant (kg^{-1}) and T is the absolute temperature (K). The thermodynamic equilibrium constant, K_o, is calculated using the equation

$$K_o = \frac{q_e}{C_e} \frac{\upsilon_s}{\upsilon_e} \tag{1.13}$$

where υ_s = activity coefficient of the adsorbed solute;

υ_e = activity coefficient of the adsorbed solute in equilibrium suspension.

The ratio of activity coefficient is assumed to be unity in the dilute range of the solutions. As the concentration of the solute in the solution approached zero, the activity coefficient approached unity and Eq. 1.13 becomes

$$\lim_{C_e \to 0} \frac{q_e}{C_e} = K_o \tag{1.14}$$

The values of K_o for the adsorption reaction are determined by plotting ln (q_e/C_e) versus q_e and extrapolation to zero q_e, as suggested by Khan and Singh [57]. The enthalpy, ΔH^o_{ads}, and the entropy, ΔS^o_{ads}, of adsorption were obtained from the slope and intercept, respectively by plotting ln K_o versus 1/T according to the Van't Hoff equation:

$$\ln K_o = \frac{\Delta S^o_{ads}}{R} \quad \frac{\Delta H^o_{ads}}{RT} \tag{1.15}$$

The Gibbs free energy change, ΔG^o_{ads}, is the driving force and the fundamental criterion of spontaneity. Physisorption, to be a spontaneous thermodynamic process, must have a negative ΔG^o_{ads} value ($\Delta G^o_{ads} < 0$). Entropy, ΔS^o_{ads}, is related to probability: the larger the entropy of a system, the greater is its statistical probability. When ΔS^o_{ads} is positive ($\Delta S^o_{ads} > 0$), spontaneity is favored. Since $\Delta G^o = \Delta H^o - T\,\Delta S^o$, ΔH^o_{ads} for physisorption must be exothermic ($\Delta H^o_{ads} < 0$). The negative value of ΔH^o_{ads} will indicate the process is exothermic and the sorption behavior may be physical in nature and can be easily reversed by supplying the heat equal to the calculated ΔH^o_{ads} value for the adsorption system. The effects of the enthalpy, entropy and temperature on spontaneity are summarized in Table 1.3 [58]:

Table 1.3: The effects of the enthalpy, entropy and temperature on spontaneity.

Enthalpy, ΔH^o_{ads}	Entropy, ΔS^o_{ads}	Outcome
(–)	(+)	Spontaneous at all temperature
(+)	(–)	Nonspontaneous regardless of temperature
(+)	(+)	Spontaneous only at high temperature
(–)	(–)	Spontaneous only at low temperature